ACS APPLIED MATERIALS & INTERFACES

Research Article

www.acsami.org

Polymer Stabilized Fe_3O_4-Graphene as an Amphiphilic Drug Carrier for Thermo-Chemotherapy of Cancer

Akshaya Kumar Swain,[†,∥] Lina Pradhan,[‡,∥] and Dhirendra Bahadur*[,§]

[†]IITB-Monash Research Academy, Department of Metallurgical Engineering and Materials Science, Indian Institute of Technology-Bombay, Mumbai, Maharashtra, India, 400076

[‡]Center for Research in Nanotechnology and Science, Indian Institute of Technology-Bombay, Mumbai, Maharashtra, India, 400076

[§]Department of Metallurgical Engineering and Materials Science, Indian Institute of Technology-Bombay, Mumbai, Maharashtra, India, 400076

Supporting Information

ABSTRACT: In light of the growing interest in the search for cheap and effective solutions for cancer treatment, we report a simple one pot synthesis of polymer stabilized iron oxide-graphene (PIG) that could be realized on a large scale. The structural (Fe_3O_4 particle size of ∼11 nm), functional (various oxygen containing moieties), and magnetic (moment of ∼43 emu/g) properties of PIG are explored using various characterization techniques for possible biomedical applications. PIG shows good colloidal stability and is biocompatible even at higher concentrations (2.5 mg/mL) by virtue of cross-linking polymers. The biocompatibility of the composite has been tested using HeLa cell lines by computing the percentage of the reactive oxygen species through the 2,7-dichlorofluorescein (DCF) intensity level. PIG has the ability to load and release both hydrophobic and hydrophilic drugs with a good loading efficiency and capacity. The dug loading efficiency of PIG is measured to be ∼87% and ∼91% for doxorubicin (DOX) and paclitaxel (PTXL), respectively. Under an AC magnetic field, superparamagnetic PIG (2.5 mg/mL) takes less than 16 min to reach the stable hyperthermia temperature, suggesting it as a good anticancer material. A time-dependent cellular uptake of doxorubicin-conjugated PIG has been studied to optimize the parameters for thermo-chemotherapy of cancer. The synergetic effect of both the drug and hyperthermia is observed in the killing of the cancerous cells, verified by computing the cell apoptotic population using a flow cytometer. However, it has been noticed that, even in the absence of chemotherapy, PIG shows good antiproliferative activity with thermotherapy alone.

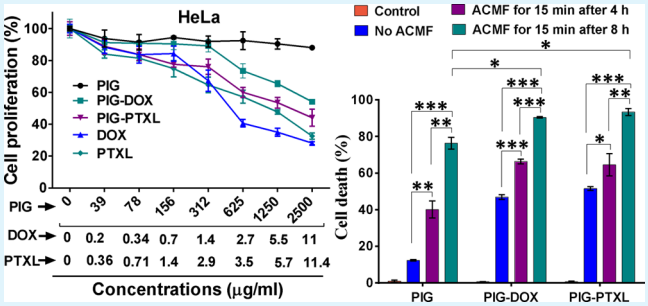

KEYWORDS: *cancer, drug carrier, graphene, iron oxide, stability, thermo-chemotherapy*

INTRODUCTION

There have been continuous endeavors by the researchers to develop effective therapeutic agents for the treatment of cancer.[1−3] Thus, it is customary to design functional nanocomposites by modifying its physiochemical properties, resulting in synergetic effects, in order to obtain new characteristics that are not present in its individual components alone.[4] Also, the composite materials can be tuned to accommodate the desired properties. Recently, iron oxide-carbon composites have drawn much attention due to their numerous applications in various fields, such as biomedical, energy, catalytic, environmental, and the like; iron oxide is useful for diagnostic and/or theranostic applications.[5] At the same time, graphene has intrigued the researchers with its superlative properties relevant to potential applications.[3] Amphiphilic graphene has a higher surface area compared to other nanomaterials. Every atom on its surface is vulnerable to interactions because its free π-electron is oriented in a perpendicular direction. These properties make it a potential candidate for drug delivery applications.[6] Even though the effective surface area of a multilayered graphene structure decreases, the rigidity that is required for cell penetration increases.[7] The chemistry of graphene allows it to be functionalized easily to form suitable derivatives for potential applications. Thus, the two-dimensional planar geometry of graphene with sp^2-bonded carbon atoms is a suitable platform to immobilize various atoms or molecules including cells. The inability of graphene to generate a hyperthermia temperature under an AC magnetic field (ACMF) limits its possibilities as a thermo-therapeutic agent. Thus, an alternative approach, which combines the properties of graphene and iron oxide (Fe_3O_4), has generated enormous interest in several biomedical applications.[8−13]

Received: January 12, 2015
Accepted: March 30, 2015
Published: March 30, 2015

DOI: 10.1021/acsami.5b02536
ACS Appl. Mater. Interfaces 2015, 7, 8013−8022

Despite many unique physiochemical properties, the composite (iron oxide-graphene) suffers from serious challenges. The critical drawbacks of forming this new system are cell toxicity, low colloidal stability, suppression of magnetization, and the like. These properties are essential for realizing various biomedical applications. There have been continuous efforts in addressing these challenges. Also, loading the carriers with both hydrophilic and hydrophobic drugs for versatile applications is another challenge.[14] Efficient nanocarriers should not only have the capability of a good loading capacity for any kind of drug but also should be able to make a controlled release. Moreover, it should be able to generate local heat through hyperthermia to achieve an appreciable efficiency in the killing of cancerous cells. Furthermore, if these carriers acquire the ability to be used as a magnetic resonance imaging (MRI) contrast, it would be an added advantage. Keeping the above-mentioned problems/requirements in mind, we have designed a new protocol to synthesize a polymer stabilized iron oxide-graphene (PIG) composite that is highly stable and biocompatible even at higher concentrations (2.5 mg/mL) with high magnetization (43 emu/g) values. The composite is prepared by a one pot solvothermal process. The colloidal stability and biocompatibility of PIG is achieved by adopting two cross-linking polymers.[15] The zeta potential for the PIG was measured to be ∼−25 mV. We have also demonstrated the possibility of loading both hydrophilic and hydrophobic drugs with better loading efficiency and capacity. Although PIG behaves as a good anticancer material through chemo-thermotherapy of cancer, it has a good response to thermotherapy of cancer alone as well. We expect that PIG would be a good MRI contrast agent due to the presence of polyvinylpyrrolidone (PVP) and iron-oxide in it.[16]

EXPERIMENTAL SECTION

Materials and Methods. Natural graphite powder (purity of >99.99%, average particle size of <45 μm, purchased from Sigma−Aldrich, CAS no. 7782-42-5), PVP (product no. 39765, M_r of ∼14 000, LR grade, purchased from SD Fine-Chem Limited), and poly(vinyl alcohol) (PVA) (product no. 40573, M_r of ∼(111.15)n, K30 grade, purchased from S D Fine-Chem Limited) were used as-received. The molar masses of the repeat units in PVP and PVA are 111 and 44 g/mol, respectively. Iron(III) chloride hexahydrate ($FeCl_3{\cdot}6H_2O$), iron(II) chloride tetrahydrate ($FeCl_2{\cdot}4H_2O$), doxorubicin hydrochloride (DOX·HCl), and paclitaxel (PTXL) were purchased from Sigma-Aldrich and were used as-received. Ethylene glycol (EG), sodium acetate (NaAc), and anhydrous ethanol were purchased from Merck. De-ionized (DI) water was used throughout the experiments as required.

525 mg of graphite, 2 g of PVP, and 2 g of PVA were mixed into 90 mL of DI water. Fe^{3+} (1.332 g), Fe^{2+} (0.669 g), and NaAc (4 g) were separately mixed into 60 mL of DI water. Further, the two mixtures mentioned above were mixed and stirred at 600 rpm (at room temperature). This was then transferred to an automated autoclave. First, this mixture was heated to 100 °C for 1 h (the pressure was 2 bar) with stirring. Then, the temperature was raised to 275 °C and maintained for 16 h (the pressure was 53.4 bar) with stirring. Finally, the temperature was again raised to 300 °C and kept for 8 h without stirring (the pressure was 80 bar). The autoclave was autocooled to room temperature after which the materials were washed with water and ethanol using a magnet. The obtained powder (PIG) was dried at 40−45 °C.

1. Preparation of Hydrophilic and Hydrophobic Drug Loaded PIG. Anticancer drugs such as doxorubicin (DOX) and PTXL were chosen to prepare hydrophilic (water-soluble DOX·HCl) and hydrophobic (PTXL) drug loaded PIG. Drug loading was done in a water bath by a simple mixing and overnight shaking method. Briefly, 10 mg of PIG was dispersed in 1 mL of phosphate buffer saline (PBS, pH 7.4), and then, 50 μg (per 1 mL) of DOX or PTXL was mixed with the PIG solution in a centrifuge tube (2 mL) separately. The resulting suspension was then placed overnight in a water bath shaker in the dark. Unbound DOX and PTXL supernatant were collected from the material by centrifuging at 10 000 rpm for 10 min. The obtained DOX and PTXL conjugated PIG (PIG-DOX/PTXL) was stored at 4 °C for future use. By using the calibration curves of DOX and PTXL at 490 and 230 nm, respectively, the concentration of both the drugs in the supernatants was calculated. The percentage of entrapment efficiency and loading capacity was calculated using the following relation.[17,18]

$$\text{entrapment efficiency}\ (\%) = \frac{\text{weight of drug in PIG}}{\text{weight of drug fed initially}} \times 100 \quad (1)$$

$$\text{loading capacity}\,(\%) = \frac{\text{weight of drug in PIG}}{\text{weight of PIG}} \times 100 \quad (2)$$

2. pH-Responsive and Stimuli Effect Drug Release from PIG-DOX and PIG-PTXL. The pH responsive drug release behavior of DOX from PIG-DOX and PTXL from PIG-PTXL was studied using the dialysis method. The stimuli effect of the drug release pattern of DOX and PTXL was obtained by an external ACMF. For *in vitro* release studies, 5 mg of PIG-DOX and PIG-PTXL was suspended in 1 mL of PBS at pH 7.4 (which can be compared to normal body fluids) and pH 4.3 (an acidic environment), respectively. Then, 1 mL of suspension was transferred to a dialysis bag which was placed in a beaker that contained 20 mL of PBS and stirred at 37 °C. At periodic intervals, 1 mL of the released medium was collected for evaluation of the released drug. Subsequently, 1 mL of fresh buffered solution was injected into the PBS solution to keep the total volume constant. The release efficiency of DOX and PTXL was quantified using UV−visible spectroscopy.[18] The steps mentioned above were repeated at least three times.

3. Concentration-Dependent Specific Absorption Rate (SAR) Study of PIG. The temperature rise of magnetic PIG nanoparticles was measured by applying an ACMF (418 Oe, 250 kHz). The samples (1, 2, 2.5, and 3 mg of PIG) were dispersed in 1 mL of aqueous media in a 2 mL eppendorf tube and exposed to ACMF. The rise in the temperature of each sample was recorded after every minute. The SAR values of the dispersed sample can be determined using the following equation:

$$\text{SAR} = C \times \frac{\Delta T}{\Delta t} \times \frac{1}{m_{\text{mag}}} \quad (3)$$

where C is the specific heat capacity of water (C_{water} = 4.186 J/g K), $\Delta T/\Delta t$ is the initial slope of the time-dependent temperature curve, and m_{mag} is considered to be the mass fraction of magnetic materials present in the sample.[19]

4. Cell Viability Assay. The sulforhodamine B (SRB; Sigma-Aldrich) assay was carried out to evaluate the proliferative activity of the PIG, PIG-DOX, and PIG-PTXL. The human cervical cancer (HeLa) cell line was purchased from the National Centre for Cell Sciences (NCCS-Pune, India). The cells were cultured in a DMEM medium supplemented with 10% fetal brovine serum (FBS; Hi-Media, Mumbai, India) and a 1% antibiotic antimycotic solution (Hi-Media, Mumbai, India) that was placed in a humidified incubator at 37 °C and 5% CO_2. To quantify cell viability, HeLa cells were cultured at a density of 1×10^4 cells/well in 96-well plates at 37 °C. After overnight incubation, the cells were treated with different concentrations of PIG, PIG-DOX, and PIG-PTXL for 24 h. Then, the treated plates were processed for the SRB assay.[20] For viability measurement, the absorbance was measured at λ_{abs} = 560 nm using a microplate reader and computed using the following formula:

$$\text{cell viability}\ (\%) = \frac{\text{absorbance of treated cells}}{\text{absorbance of control}} \times 100 \quad (4)$$

DOI: 10.1021/acsami.5b02536
ACS Appl. Mater. Interfaces 2015, 7, 8013−8022

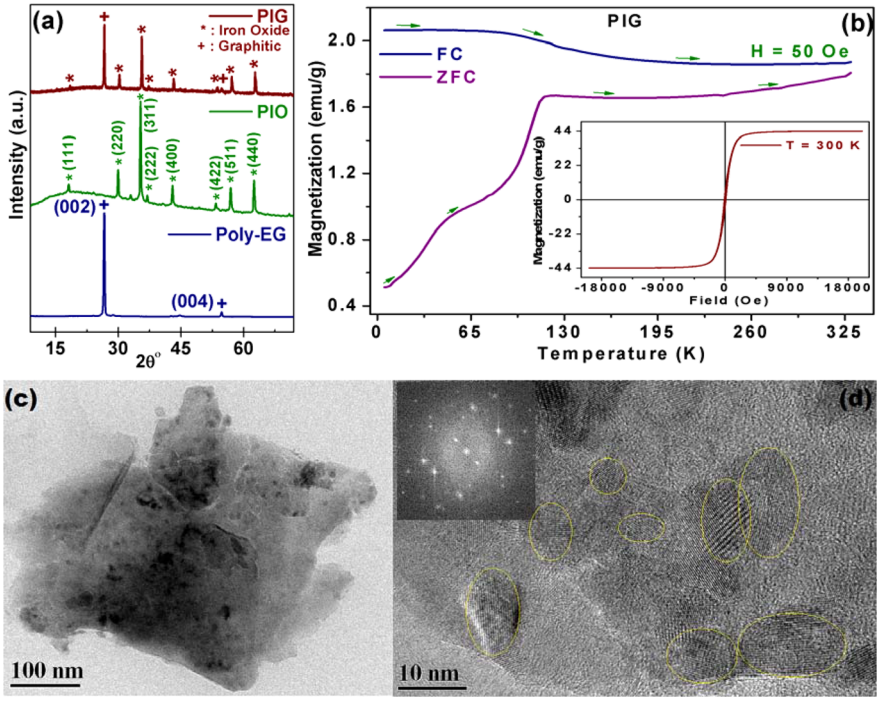

Figure 1. (a) Comparison of XRD plots of poly-EG, PIO, and PIG, (b) ZFC-FC plot of PIG. The inset in (b) shows the *m* versus *H* plot of PIG. (c) TEM image of PIG and (d) HR-TEM image of PIG showing both graphene sheets and iron oxide nanoparticles. The inset in (d) shows the FFT view of the HR-TEM image. Iron oxide nanoparticles are also present in between the graphene sheets.

5. Time-Dependent Cellular Uptake of PIG-DOX. The time-dependent cellular uptake of DOX-loaded PIG nanoparticles was determined by confocal microscopic imaging techniques. For time-dependent cellular uptake studies, 1×10^4 HeLa cells were seeded on coverslips in 24 well plates filled with DMEM media. The plates were transferred to an incubator (which was maintained at 37 °C and 5% CO_2) for a night. The cultured cells were then treated with PIG-DOX (0.25 mg/mL). After incubation for different periods (4, 8, and 24 h), the treated cells were washed with sterile PBS for three times at least. The coverslips with the attached cells were fixed with 4% paraformaldehyde for 10 min at room temperature. Further, the coverslips were washed with PBS to remove the extra fixing agents and then mounted onto a glass slide for imaging. Fluorescent images of the prepared slides were taken by a 3i Olympus Spinning Disk Confocal Microscope (488 nm laser). The fluorescent characteristic of DOX (λ_{ex} = 470 nm, λ_{em} = 590 nm) was used to monitor the cell uptake of PIG-DOX at 4, 8, and 24 h.[21]

6. Determination of Cellular Reactive Oxygen Species (ROS) Level. The cellular ROS production was measured by spectrofluorometry using an ROS detecting reagent, 2,7-dichlorodihydrofluorescein diacetate (DCFH-DA, purchased from Sigma), which is membrane permeable and trapped intracellularly following deacetylation. The DCFH-DA reacts with several ROS (H_2O_2, hydroxyl radical, peroxyl radical, and the like) in the cellular compartment to produce the oxidized fluorescent form 2,7-dichlorofluorescein (DCF) which emits green fluorescence. Briefly, a 10 mM DCFH-DA stock solution was prepared in dimethyl sulfoxide (DMSO) and diluted in DMEM to obtain a 10 μM working solution. The density of 1×10^4cells per well were seeded in the 96-well plates and incubated overnight in the incubator. Then, the cells were treated with PIG, PIG-DOX, and PIG-PTXL at different concentrations and incubated for 24 h subsequently. The treated cells were washed twice with PBS followed by addition of a 10 μM working solution of DCFH-DA with fresh media at 37 °C for 1 h. Finally, cells were washed twice with chilled PBS and resuspended in the same buffer. The intracellular ROS production was measured using a reader plate at an excitation wavelength of 485 nm and an emission wavelength of 535 nm.[22,23]

7. Synergistic Effect of PIG-DOX and PIG-PTXL Treatment in Comparison to PIG Treatment. To quantify cell death efficiency, HeLa cells were seeded at a density of ~1×10^6 with 1 mL of completed DMEM media in a 30 mm Petri plate. After overnight culturing, the cells were treated with 2.5 mg/mL of PIG, PIG-DOX, and PIG-PTXL. For combined treatments, the PIG-DOX and PIG-PTXL-treated cell plates were incubated for 4−8 h in an incubator. After incubation for different periods, one set of treated cell (in triplicate) plates was exposed to ACMF (at 418 Oe, 250 kHz) for 15 min at 42 °C and then transferred to an incubator overnight. Another set of treated plates was kept overnight in an incubator without applying any ACMF. Cell death efficiency was determined using trypan blue dye exclusion.[24]

8. Cell Cycle Distribution and Apoptotic Analysis by Flow Cytometer. Cells were seeded at a density of ~1×10^6 cells in a 30 mm Petri dish and incubated overnight at 37 °C in an incubator containing 5% of CO_2. 2.5 mg/mL of PIG, PIG-DOX, and PIG-PTXL was added to the cells and incubated for 4 h. The samples were exposed to an ACMF for 15 min and then transferred to the incubator for 24 h. After removing the media, the cell pellet was collected by centrifugation. Samples were prepared for cell cycle analysis and its apoptosis population. For cell cycle distribution, the cell pellet was fixed with 70% chilled ethanol overnight at 4 °C followed by addition of 10 μg/mL of RNase A and stained with 50 μg/mL of propidium iodide (PI) for 30 min.[24] For each sample 10 000 cells were counted using a flow cytometer (BD FACS Callibur). The histograms were analyzed by Motif software.

9. Statistical Analysis. Each experiment was carried out in triplicate and over three different times at least. Data is expressed as mean ± standard deviation (SD). The statistical analysis was determined by an unpaired two-tailed *t* test using the GraphPad-6 Prism software. Significant differences between values are denoted as follows: * (p < 0.05), ** (p < 0.01), and *** (p < 0.001).

RESULTS AND DISCUSSION

The Making of PIG. Previously, we have reported that graphite can be exfoliated at high temperature and pressure.[25] The polymers (PVP and PVA) have the ability to cross-link and, thus, may get wrapped onto the exfoliated graphene sheets via van der Waals forces and/or H-bonding.[26] The wrapping of

DOI: 10.1021/acsami.5b02536
ACS Appl. Mater. Interfaces 2015, 7, 8013−8022

polymer onto graphene sheets can be seen from the transmission electron microscopy (TEM) images given in Figure S1 in the Supporting Information. However, upon removing this high temperature and pressure, the graphitic structure may recover partially. Thus, one can obtain exfoliated graphite that would have polymeric interactions with the cross-linking polymers. The formation of graphene sheets (few layer) can be easily seen from the TEM images given in Figure S2 in the Supporting Information. Further, the formation of iron oxide nanoparticles by using the polymers (PVP and PVA) to enhance the colloidal stability and biocompatibility of the composite is explored. However, PVP may also act as a mild reducing agent and may assist in attaching the Fe_3O_4 nanoparticles on the graphene surface.[27] NaAc, which was part of the synthesis process, may also act as a reducing agent. Thus, the kinetics of the nanoparticles formation may get affected as well. We expect the formation of variable sizes of anisotropic nanoparticles due to the occurrence of more than one reducing agent. Finally, the polymers also help in depositing the nanoparticles on the surface of the graphene.[7]

The X-ray diffraction (XRD) pattern of polymer exfoliated graphite (poly-EG) is shown in Figure 1a.[25] The formation of Fe_3O_4 is also separately confirmed by adding two cross-linking polymers to the iron oxide precursors, and its (PIO: polymer-iron oxide) XRD pattern is presented in Figure 1a. After having learned of the possibility of the formation of poly-EG and PIO by polymers, we combined the above protocols for an *in situ* synthesis of PIG. The XRD plot of PIG as shown in Figure 1a supports the presence and formation of both Fe_3O_4 and graphene sheets in PIG. We observe a spinel structure of the magnetic nanoparticles. The average crystallite size of magnetic nanoparticles computed from the (311) peak was found to be ~11 nm, by using the Scherrer formula. The Fe_3O_4 diffraction peaks in PIG were found to have a small shift (~0.2°) with that compared to the data of the International Center for Diffraction Data (Reference Code: 00-001-1111). This confirms no change in the phase of Fe_3O_4 nanoparticles present in PIG. It should be noted that the graphene in PIG are not necessarily single layers, rather these are few layered graphene sheets.

The iron oxide in PIG is responsible for its magnetization. The composite was found to be superparamagnetic with a magnetization value of ~43 emu/g (inset of Figure 1b). The zero field cooled-field cooled (ZFC-FC) data of PIG at an applied field of 50 Oe is presented in Figure 1b. The formation of Fe_3O_4 can also be verified from the presence of the Verwey transition at ~120 K in the ZFC-FC plot.

The TEM and high resolution-TEM (HRTEM) image of PIG is given in Figure 1c,d. The inset shows the fast Fourier transform (FFT) view of the HR-TEM image. The micrograph shows a partially agglomerated morphology with a variable particle size. This is due to the presence of excess PVP that is absorbed on Fe_3O_4 surfaces.[28] The backbone of the PVP contains hydrophobic carbon chains and polar lactams which assist in the adsorption process. The PVP molecules facilitate a self-assembly process by reducing the surface energy of the system through van der Waals forces between the particles. Also, the presence of graphene polymer as the base material further assists in keeping the nanoparticles intact by virtue of a higher surface energy on the surface of the Fe_3O_4 nanoparticles.[7] A similar behavior can be seen in silica in the presence of protein or lipid layers. A fraction of iron oxide nanoparticles was also found to be present in between the few-layer graphene sheets. The same behavior can also be seen from the HR-TEM image of PIG. The average size of iron oxide nanoparticles and graphene sheets in PIG (calculated from TEM images) was computed to be ~14.5 ± 3.2 and 500 nm, respectively. The size distribution is presented in Figures S3 and S4 in the Supporting Information. Due to a larger size of the carrier (graphene sheets), we anticipate that PIG is suitable for intratumoral methods of injecting the drug loaded carrier.

The FTIR spectra of PIG in the range of 400−4000 cm^{-1} is shown in the inset of Figure 2. The presence of Fe−O bonds in

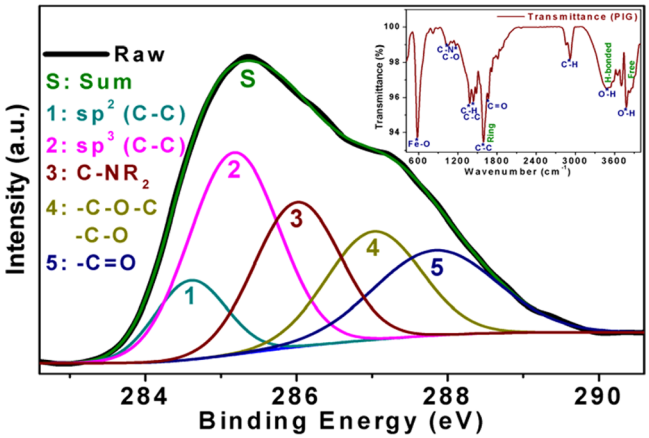

Figure 2. Both XPS and FTIR (shown in the inset) of PIG support the presence of multifunctional moieties that enables the binding of hydrophobic and hydrophilic drugs.

Fe_3O_4 (in PIG) is evident from the broad and strong absorption peak at ~577 cm^{-1}. The broad peak at ~3400−3600 cm^{-1} reveals the presence of an H-bonded O−H stretching vibration that enhances the hydrophilic nature of the composite. The band, around ~3780 cm^{-1}, signifies the free O−H bonds in PIG which may further help in getting the drug molecules attached to these sites. The presence of C−H and C−N vibrations at ~830 and 1047 cm^{-1}, respectively, represents the linking of PVP to the surface of other molecules.[7] Several other major vibrations (C−C, C═O, C−O) were observed in the PIG that represents the various interactions in PIG. To further cement the FTIR observations, XPS studies were performed. The C 1s spectra presented in Figure 2 justifies the fact that PIG is functionalized. It can be seen that sp^3 bonding in C−C dominates. This behavior is quite common in composites of graphene/graphene oxide. It suggests an interaction between the graphene sheets and the surrounding molecules.[15] Thus, we find that the FTIR and XPS results are complementary to each other. This confirms the presence of various functional groups in the composite that helps to bind with any foreign or drug molecule through their active sites resulting in a well-dispersed suspension.

1. Evaluation of Drug (DOX and PTXL) Loading Efficiency. PIG that consists of hydrophilic polymers (PVP/PVA) and hydrophobic sp^2 carbon sheets are amphiphilic in nature. Thus, a higher loading capacity and loading efficiency of both the DOX and PTXL drugs are seen. The surface and edges of the graphene sheets in PIG are functionalized by various functional groups (C═O, C−O−C, C−O, C−NR_2, etc.). These functional groups can easily bond with OH and NH_2 groups in DOX and PTXL by virtue of $\pi-\pi$ and/or the hydrophobic interactions between them. The drug loading behavior of PIG was evaluated by a UV−visible spectrometer.[29] Figure 3a shows

DOI: 10.1021/acsami.5b02536
ACS Appl. Mater. Interfaces 2015, 7, 8013−8022

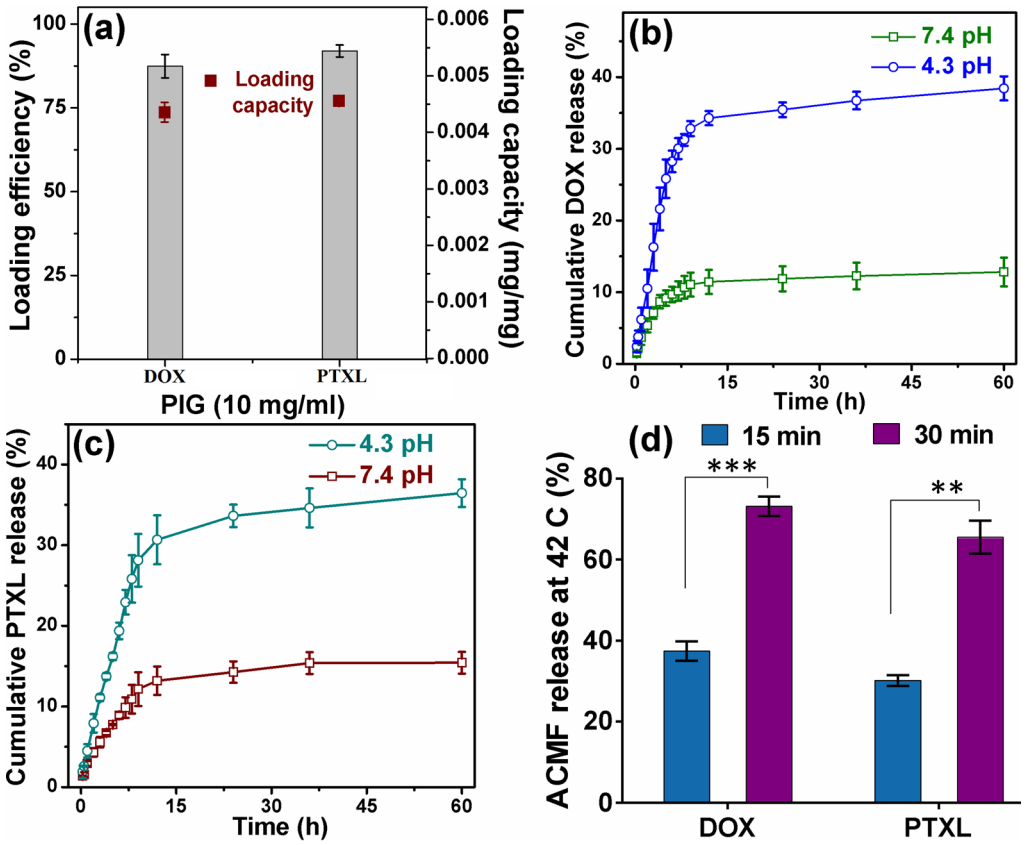

Figure 3. (a) Loading efficiency (%) and loading capacity (mg/mg) of DOX and PTXL at 10 mg/mL of PIG, (b and c) pH dependent release profiles of DOX from PIG-DOX and PTXL from PIG-PTXL, and (d) triggered drug release profiles of DOX from PIG-DOX and PTXL from PIG-PTXL at 42 °C under ACMF. The differences beteween 15 and 30 min for the DOX and PTXL release are significant at $p < 0.01$ and $p < 0.001$ as determined by an unpaired, two-tailed *t*-test. The values are expressed as mean ± SD ($n = 3$).

a higher loading efficiency of both the drugs, DOX (~87 ± 3%) and PTXL (~91 ± 2%). The drug loading capacity was estimated to be ~0.0041 and 0.005 mg/mg for DOX and PTXL, respectively. These results indicate that the physical entrapment efficiencies of both hydrophilic and hydrophobic drugs are higher due to the presence of higher active sites on the surface of PIG. The functional groups present in PIG also increase the loading level of DOX and PTXL. It has been a challenge to conjugate hydrophobic drugs due to poor solubility and hydrophobic interactions.[14] However, PIG successfully conjugates PTXL due to the presence of cross-linking polymers that overcome these problems.[15] This could also be because PIG constitutes amphiphilic graphene.

2. pH-Dependent and External Stimuli-Triggered Drug Release Studies. Figure 3b–d demonstrates the *in vitro* cumulative drug release profile of PIG at two different pH values (7.4 and 4.3) and under an external stimuli (ACMF). The release rates of DOX and PTXL are higher at an acidic environment (pH 4.3) in comparison to that of at a physiological environment (pH 7.4) over a measured period. The accumulated release efficiency of DOX and PTXL over a measured period was found to be around ~38 ± 2% and 36 ± 2% at pH 4.3 and ~13 ± 2% and 15 ± 1% at pH 7.4, respectively. The initial (within 12 h) release rate is most likely due to the rapid release of DOX and PTXL (Figure 3b,c) on the surface and near the exterior surface of PIG. Thereafter, it gradually decreases. However, the release rate at pH 4.3 after 12 h is still higher than that at pH 7.4, which might be due to their higher diffusion rates and increased protonation of functional groups (NH_2/OH) of drugs attached to PIG. Thus, the results suggest that the release of the DOX and PTXL drug release profile from PIG is highly pH dependent.[30]

Furthermore, the release profiles from drug-conjugated PIG were examined in the presence of ACMF at 42 °C. Figure 3d shows the effect of ACMF on drug release at 42 °C. The drug (DOX and PTXL) release rates in the presence of ACMF applied for 15 and 30 min were found to be ~37 ± 2% and 30 ± 1% and ~73 ± 2% and 65 ± 4%, respectively. There is a clear indication of a significantly higher release of DOX ($p < 0.001$) and PTXL ($p < 0.01$) under ACMF. This is because of the fact that the ACMF generates a strong mechanical force locally that breaks the bonds facilitating drug diffusion. Also, the soft polymer membrane (periphery) of PIG is disrupted due to the local heat generated by the magnetic particles under ACMF that enhances the drug release from PIG.[24,31]

3. Heating Ability of PIG under ACMF. Figure S5 in the Supporting Information shows the time-dependent temperature rise plots of PIG (for 1 to 3 mg/mL) under ACMF at 418 Oe (250 kHz). The heating ability was measured on the basis of the SAR value. SAR depends on certain parameters, such as the magnetic-field strength, the frequency (both kept fixed in this case), the concentration, and the suspension stability in aqueous media. It is evident that the rate of temperature rise was the fastest for 3 mg/mL of PIG than that for 1, 2, and 2.5 mg/mL of PIG dispersion. A stable hyperthermia temperature of ~42 °C was attained for a concentration of 2.5 mg/mL of PIG after application of ACMF for 15 min.

DOI: 10.1021/acsami.5b02536
ACS Appl. Mater. Interfaces 2015, 7, 8013–8022

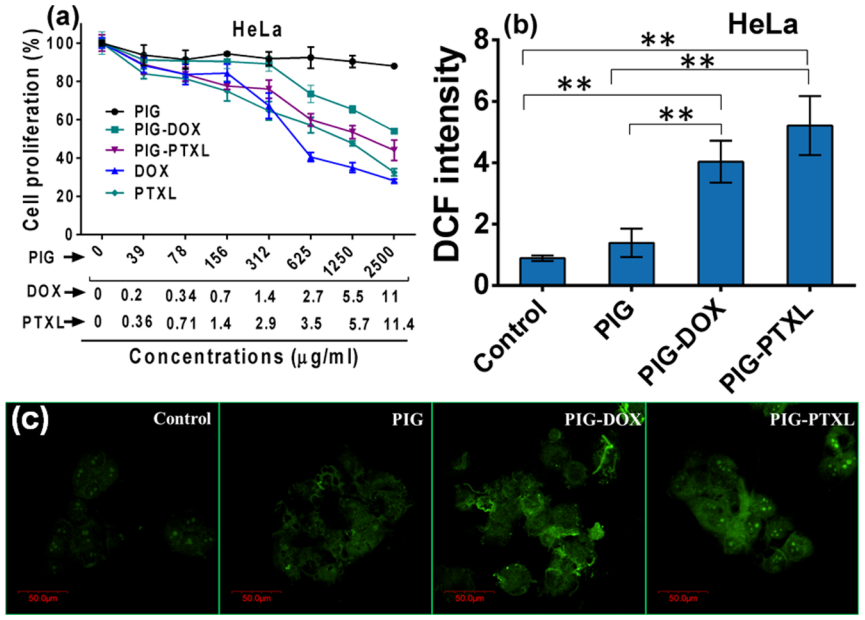

Figure 4. (a) Relative cell proliferation effect of PIG, PIG-DOX, PIG-PTXL, DOX, and PTXL up to 2.5 mg/mL (2500 μg/mL) with various concentrations of drug contents after 24 h in HeLa cells. (b) Quantification of intracellular ROS levels in HeLa cells after treatment of PIG, PIG-DOX, and PIG-PTXL along with untreated control (24 h incubation) as measured by DCF fluorescence ((λ_{Ex} = 485 nm; λ_{Em} = 535 nm). Relative ROS levels of PIG-DOX and PIG-PTXL are significantly higher ($p < 0.01$) compared to the untreated control and PIG treated groups (assessed by an unpaired, two-tailed *t*-test). (c) The generation of ROS using DCFH-DA in HeLa cells after exposure to PIG, PIG-DOX, PIG-PTXL, and the unexposed control by confocal laser scaning microscopy. The values are expressed as mean ± SD (n = 3).

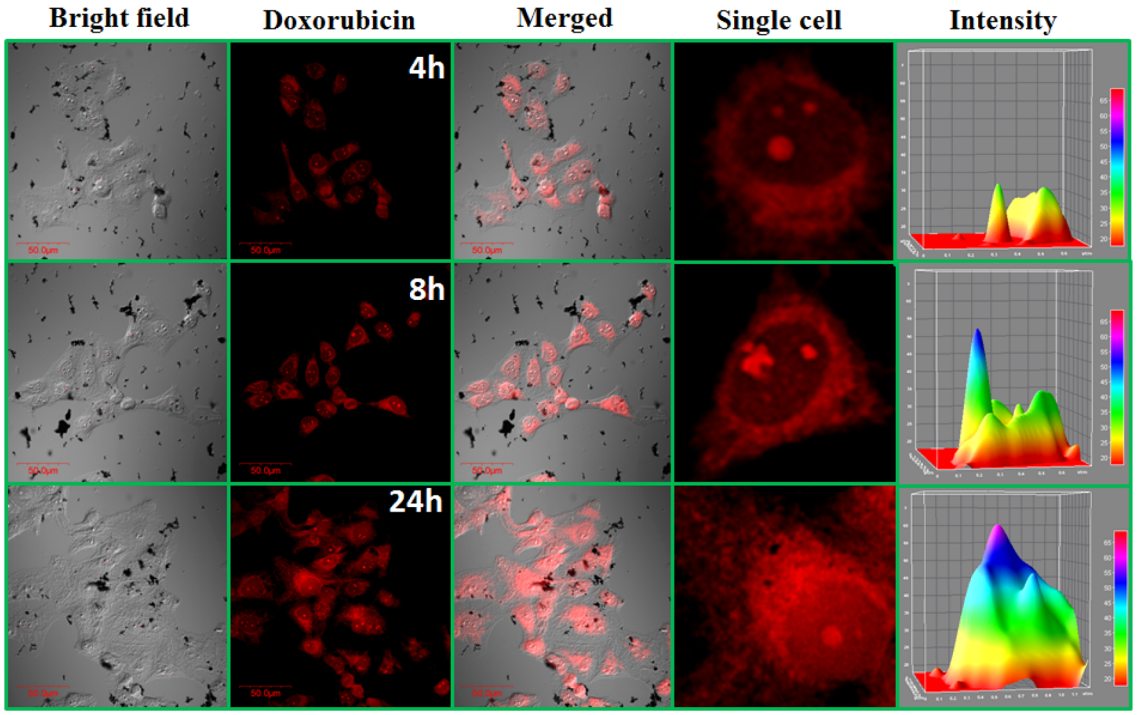

Figure 5. Determination of time dipendent intracellular uptake of PIG-DOX (red color for DOX) in HeLa cells after a 4, 8, and 24 h incubation at 37 °C using confocal laser scaning microscopy. Images show the presence of DOX, that are bound to the cytoplasm and nucleus sites with different intensity levels at different intervals. All the scale bars in the images are 50 μm.

4. Cell Viability Study. The dose-dependent cytotoxic effects of PIG and drug conjugated PIG were observed on the HeLa cell line and shown in Figure 4a. It is observed that even at a higher material concentration (2.5 mg/mL), PIG showed cell viability that is greater than 80% after a 24 h incubation. This result indicates good cell compatibility in PIG. However, inhibition of cell proliferation was observed when the cells were treated with PIG-DOX, PIG-PTXL, free DOX, and free PTXL at different doses for 24 h. As shown in Figure 4a, cytotoxicity of PIG-DOX and PIG-PTXL was found to be ~54 ± 1% and 44 ± 5%, respectively, at 2.5 mg/mL (~5.8 μg/mL of DOX and 14 μg/mL of PTXL) after 24 h. In comparison to free drugs,

DOI: 10.1021/acsami.5b02536
ACS Appl. Mater. Interfaces 2015, 7, 8013−8022

PIG-DOX and PIG-PTXL showed lower cytotoxicity due to the gradual release of DOX and PTXL within the cells.

5. Measurement of Intracellular Reactive Oxygen Species (ROS) Level. It is reported that oxidative stress is one of the proposed mechanisms of cellular cytotoxicity related to nanoparticle interaction.[32,33] The ROS generation is involved in the cytotoxicity of cells without any drugs and drug-conjugated nanoparticles exposed to the cells. A significant ($p < 0.01$) increase in the intercellular levels of ROS by PIG-DOX (~4 ± 1) and PIG-PTXL (~5 ± 1) was observed at a 0.5 mg/mL concentration relative to the untreated control cells, as shown in Figure 4b. The ROS level of PIG was found to be reduced when compared to that of drug-conjugated PIG (~1 ± 0.5) at 0.25 mg/mL (Figure 4b). These results show that the PIG-treated cells increase the cell viability by decreasing the cellular ROS level, while PIG-DOX and PIG-PTXL induce toxicity by increasing the cellular ROS level. There is no significant difference between the cells exposed to PIG and the untreated control. A higher ROS level in cells is a potential reason for cell death that is mediated by drug-conjugated nanoparticles.

The accumulation of intracellular ROS generation was confirmed by confocal microscopy of HeLa cells. Figure 4c shows the ROS production of PIG, PIG-DOX, and PIG-PTXL-treated cells using DCFH-DA staining which oxidizes to form the DCF green fluorescence.[34] In contrast, PIG treated cells show a lower amount of higher ROS generation level as compared to the untreated control group. Intriguingly, the intensity of fluorescence increased in the presence of PIG-DOX and PIG-PTXL at 0.5 mg/mL concentration in the cells compared to that of the PIG group. These results reassert that the release of drug molecules from PIG induces a higher ROS level and facilitates the increase of the cytotoxic effect of HeLa cells.

6. Time-Dependent Cellular Uptake of PIG-DOX. We monitored the internalization process of PIG-DOX nanoparticles using a confocal microscope. According to this study, the accumulation of PIG-DOX in HeLa cells depends on time. Figure 5 shows PIG-DOX accumulated in the cells in a time dependent manner after 4 h of treatment. As the incubation time was increased, the DOX fluorescence (red color) became more intense inside the cells and was evenly distributed in the cytoplasm (at 24 h). The increase in the intensity of the images indicates that PIG-DOX was taken up within 24 h by the cells and localized in the cytoplasm and nucleus region. The mechanism responsible for the internalization of PIG-DOX is considered to be a cell membrane−nanoparticle interaction and the penetration of cell membrane by nanoparticles. These results indicate that the uptake of PIG-DOX by HeLa cells was highly dependent on the incubation time. After 8 h, the release of the drug gradually increased inside the cytoplasm and the nucleus site which may have increased the cytotoxic effect of cells.

7. Synergistic Effect of PIG-DOX and PIG-PTXL (Drug and Hyperthermia) Treatment Compared to PIG Treatment. PIG with high thermal absorbance properties and an efficient drug loading capacity was prepared for thermo-chemotherapy studies. The presence of cross-linking polymers in PIG increases the colloidal stability thereby facilitating more internalization in the cells by an enhanced permeation and retention (EPR) effect.[35] A simultaneous cytotoxic effect due to hyperthermia and chemotherapy in PIG, PIG-DOX, and PIG-PTXL (2.5 mg/mL) has been evaluated under an applied ACMF. It took 900 s to reach the hyperthermia temperature (~42 °C) at 418 Oe (250 kHz). Upon a 15 min exposure to ACMF, ~40 ± 4% ($p < 0.01$) and ~76 ± 3% ($p < 0.001$) cell death was observed after a 4 and 8 h incubation of PIG with cells, respectively, when compared to no ACMF exposure (~12 ± 1%). This is presented in Figure 6. Combined hyperthermia

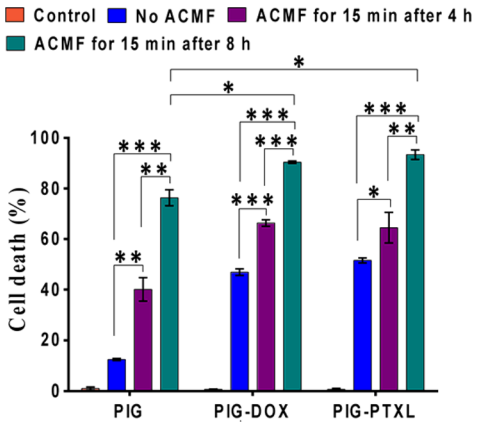

Figure 6. The cell death efficiency of HeLa cells with 2.5 mg/mL of PIG, PIG-DOX, and PIG-PTXL, which are incubated for 4 and 8 h. Then, one set of treated plates are exposed to ACMF (at 418 Oe, 250 kHz) for 15 min at 42 °C and another set is retained (in the absence of ACMF). After only PIG, PIG-DOX, and PIG-PTXL treatment in the presence/absence of ACMF and untreated control, all groups are incubated for 24 h at 37 °C. For each group, differences between no ACMF and ACMF groups for 4 and 8 h are significant at $p < 0.05$, $p < 0.01$, and $p < 0.001$. The cell death % is significantly higher ($p < 0.01$ and $p < 0.001$) after an 8 h uptake compared to 4 h. The cell death % with treatment of PIG-DOX and PIG-PTXL under ACMF is significantly higher ($p < 0.05$) compared to PIG treatment under ACMF. All results are determined by an unpaired, two-tailed *t*-test. The values are expressed as mean ± SD ($n = 3$).

and drug enhanced cell death by ~66 ± 1% ($p < 0.001$) and 90 ± 1% ($p < 0.001$) and ~64 ± 6% ($p < 0.05$) and 93 ± 1% ($p < 0.001$) after a 4 and 8 h incubation of PIG-DOX and PIG-PTXL, respectively, in comparison to that of no ACMF exposure (~47 ± 1% and 51 ± 1%). Synergistically, hyperthermia with drug treatment is much more effective and enhances the cytotoxicity of PIG-DOX and PIG-PTXL; this is because the cell death could be due to necrosis or apoptosis with local heat generation and more drug release by ACMF.[24,36,37] In order to understand the mechanism of the combined therapy of hyperthermia and drug treatment in destroying cancer cells, further studies were performed and are discussed below.

Morphological studies were performed on HeLa cells in the presence and absence of ACMF. Figure 7 shows microscopic images of HeLa cells after treatment with PIG, PIG-DOX, and PIG-PTXL in the presence/absence of ACMF monitored for 24 h incubation. In all cases, control cells are untreated in Figure 7a−c. Figure 7d shows no significant changes in cellular morphology after PIG treatment. Figure 7e,f shows the effect of PIG-DOX and PIG-PTXL in the absence of ACMF. In both cases, the cellular morphology was rounded for drug releases from PIG. Figure 7g−i shows more rounding of cells in the morphology (after a 4 h incubation) under ACMF compared to that without ACMF. Also, it was observed that most of the cells were rounded when the treated cells were incubated for 8 h and then exposed to ACMF for 15 min at 42 °C (Figure 7i−k).

DOI: 10.1021/acsami.5b02536
ACS Appl. Mater. Interfaces 2015, 7, 8013−8022

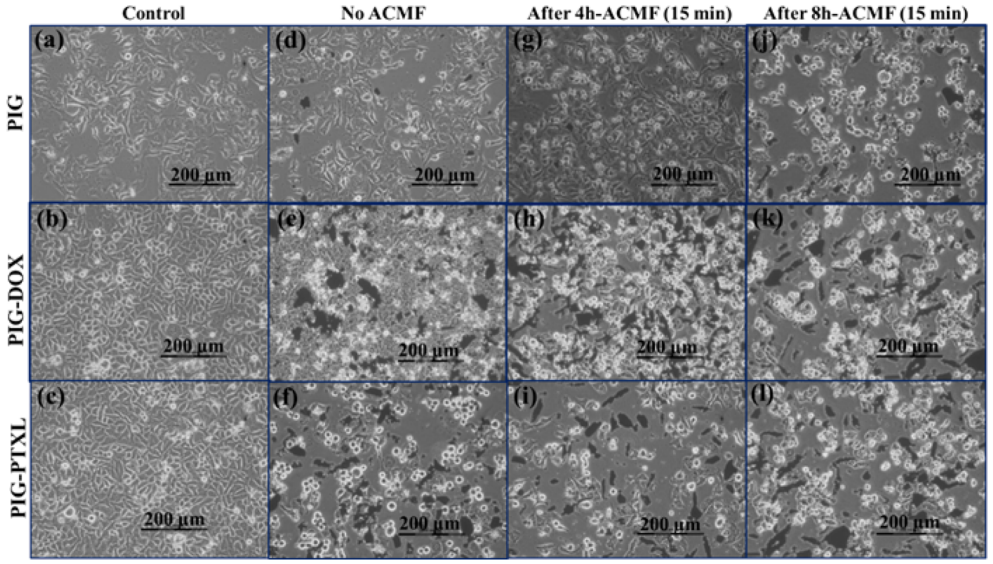

Figure 7. Optical microscopic images of HeLa cells: (a–c) Untreated control, (d–f) after treatment with PIG, PIG-DOX, and PIG-PTXL in the absence of ACMF, after a 4 h (g–i) and 8 h (j–l) incubation with PIG, PIG-DOX, and PIG-PTXL exposed to ACMF for 15 min at 42 °C and further overnight incubation. All the images have the same scale bar (200 μm).

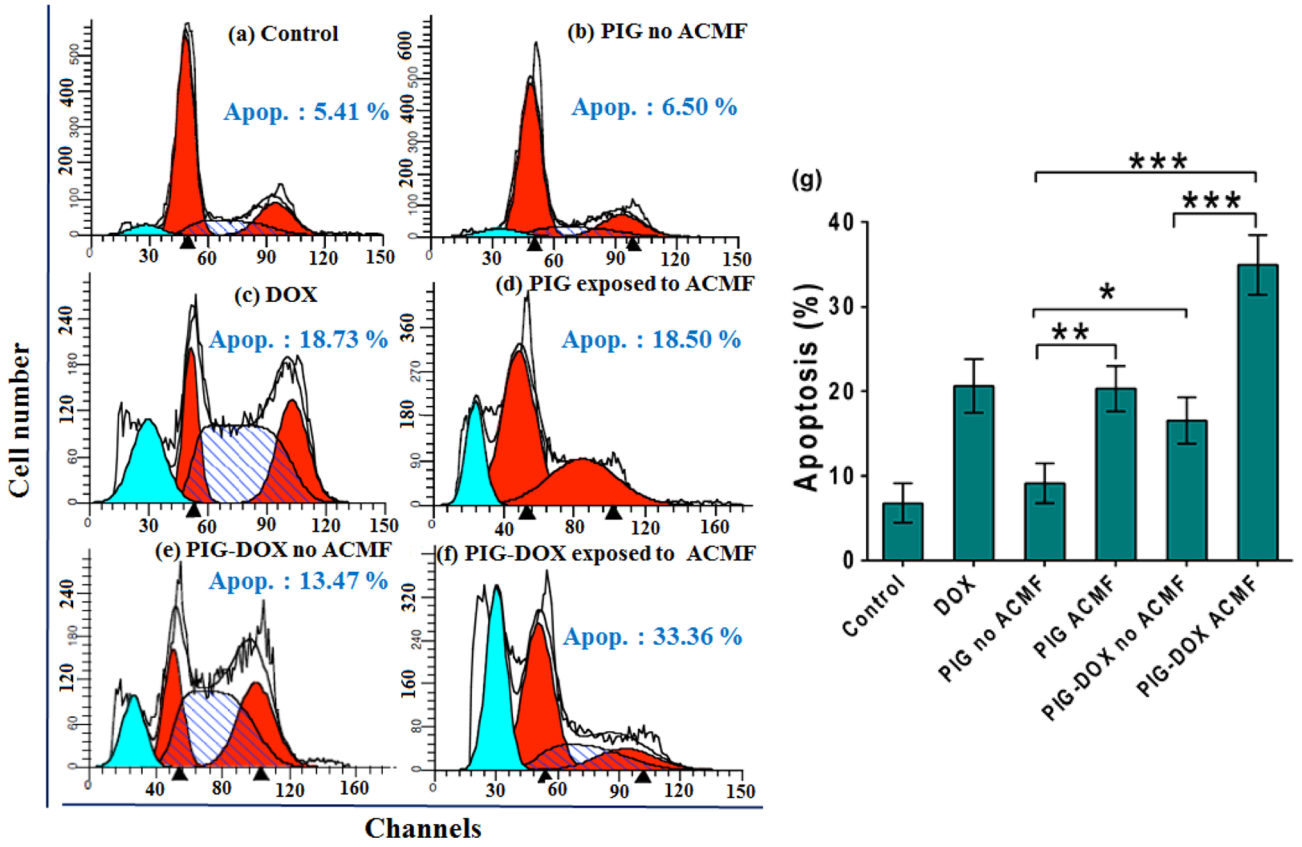

Figure 8. Flow cytometric analysis of the cell cycle distribution and apoptotic population in HeLa cells were incubated overnight after treatment (8 h incubation with materials): (a) untreated control, (b) after treatment with PIG in the absence of ACMF, (c) treated with DOX, (d) after an 8 h treatment with PIG in the presence of ACMF for 15 min at 42 °C, (e) treated with PIG-DOX with out ACMF, and (f) after an 8 h treatment with PIG-DOX exposed to ACMF for 15 min at 42 °C; (g) the percentage of apoptotic population was evaluated by flow cytometric analysis. The differences between no ACMF and ACMF of PIG treatment are significant at $p < 0.01$. The treatment of PIG-DOX in the presence of ACMF is significantly higher ($p < 0.001$) compared to PIG-DOX in the absence of ACMF. All results are determined by an unpaired, two-tailed *t*-test. The values are expressed as mean ± SD ($n = 3$).

These results show that, with increasing time for cellular uptake of drug loaded PIG, it is possible to cause maximum cell death under ACMF. Thus, local heat and drugs can directly cause significant cell membrane and DNA damage, resulting in a higher apoptotic cell death. All these results reveal that enhanced cell death is due to the synergistic effect of local

DOI: 10.1021/acsami.5b02536
ACS Appl. Mater. Interfaces 2015, 7, 8013–8022

heat generation with high intracellular uptake of nanoparticles and stimuli-triggered drug release in the cells.[24,38]

8. Cell Cycle Distribution and Apoptotic Analysis by Flow Cytometry. HeLa cells were treated with drugs and PIG (drug loaded and unloaded PIG) in the presence and absence of ACMF. Subsequently, cell cycle studies were performed by flow cytometry. The cell cycle and cell death mechanism is a complex process in which cells control the growth signals that are processed through various checkpoints. The inhibition of cell growth induces changes in the proliferation dynamics of cells. The apoptotic population rate was linked to the phase arrest of the cell cycle. Figure 8 shows different phases of the cell cycle and the apoptotic population after a 24 h treatment of cells with PIG, DOX, and PIG-DOX. Both the control (Figure 8a) and PIG-treated (Figure 8b) cells show a similar nature of growth effect. The drug (DOX) shows a more cytotoxic effect when compared with that of PIG-DOX (Figure 8c,e.). As is evident from Figure 8d,f, the cell growth inhibitory effect with PIG and PIG-DOX treated cells is higher when the treatment is performed with the drugs and under ACMF. The treatment under ACMF induces a strong G1/G2 phase arrest, significantly due to inhibition of DNA replication.[24,39] Significant changes in cell apoptosis population were observed (Figure 8g). The combined effect of the anticancer drug and the local heat significantly ($p < 0.001$) increases the cell apoptosis to ~34 ± 3% (PIG-DOX under ACMF) from ~17 ± 3% (PIG-DOX in the absence of ACMF). This is demonstrated in Figure 8g. PIG shows an apoptosis population of ~20 ± 3% under ACMF while PIG shows an apoptosis population of ~9 ± 2% without ACMF. The resulting apoptotic population of untreated control cells showed ~6 ± 2%, which is close to ~9 ± 2% of the treated PIG. These results clearly corroborate the previous biocompatibility of PIG at higher concentrations (2.5 mg/mL).

CONCLUSION

Graphene (few layers) was produced by exfoliating graphite using cross-linking polymers at a high temperature and pressure. The same route was adopted to make a polymer stabilized composite of graphene-iron oxide. PIG was found to have a high magnetization value. Also, PIG showed a good colloidal stability and biocompatibility due to the presence of the cross-linking polymers. This also enabled PIG to bind with both hydrophilic and hydrophobic drugs. A good loading efficiency and capacity with DOX and PTXL were observed. A synergistic effect of drugs and heat was observed in killing the cancerous cells. Detailed studies on ROS generation and cell apoptotic population were performed to verify the findings. In addition, the constituents of PIG makes it a suitable composite material for both therapeutic and diagnostic applications. However, the composite has an ability to kill the cancerous cells by hyperthermia alone. The synthesis protocol is facile and could be adopted for a large scale production to serve a better purpose in treating cancer.

ASSOCIATED CONTENT

Supporting Information

Materials and methods, TEM image and SAED pattern of polymer exfoliated graphite, size distribution of iron oxide and graphene sheets in PIG, temperature versus time plot of PIG under ACMF at various concentrations, zeta potential of PIG. This material is available free of charge via the Internet at http://pubs.acs.org.

AUTHOR INFORMATION

Corresponding Author

*Tel.: + 91 22 2576 7632. E-mail: dhirenb@iitb.ac.in.

Author Contributions

‖A.K.S. and L.P. contributed equally.

Notes

The authors declare no competing financial interest.

ACKNOWLEDGMENTS

The authors would like to express their gratitude to IITB-Monash Research Academy, DST-Nanomission and nanotechnology division of DEITY, government of India for their financial support.

REFERENCES

(1) Chandra, S.; Barick, K. C.; Bahadur, D. Oxide and Hybrid Nanostructures for Therapeutic Applications. *Adv. Drug Delivery Rev.* **2011**, *63*, 1267−1281.

(2) Brigger, I.; Dubernet, C.; Couvreur, P. Nanoparticles in Cancer Therapy and Diagnosis. *Adv. Drug Delivery Rev.* **2012**, *64*, 24−36.

(3) Shen, H.; Zhang, L.; Liu, M.; Zhang, Z. Biomedical Applications of Graphene. *Theranostics* **2012**, *2*, 283−294.

(4) Lu, J.; Deng, C.; Zhang, X.; Yang, P. Synthesis of Fe_3O_4/Graphene/TiO_2 Composites for the Highly Selective Enrichment of Phosphopeptides from Biological Samples. *ACS Appl. Mater. Interfaces* **2013**, *5*, 7330−7334.

(5) Tucek, J.; Kemp, K. C.; Kim, K. S.; Zboril, R. Iron-Oxide-Supported Nanocarbon in Lithium-Ion Batteries, Medical, Catalytic, and Environmental Applications. *ACS Nano* **2014**, *8*, 7571−7612.

(6) Goncalves, G.; Vila, M.; Portoles, M. T.; Vallet-Regi, M.; Gracio, J.; Marques, P. A. Nano-Graphene Oxide: A Potential Multifunctional Platform for Cancer Therapy. *Adv. Healthcare Mater.* **2013**, *2*, 1072−1090.

(7) Kumar, S. R.; Marianna, L.; Gianni, S.; Nathanael, A. J.; Hong, S. I.; Oh, T. H.; Mangalaraj, D.; Viswanathan, C.; Ponpandian, N. Hydrophilic Polymer Coated Monodispersed Fe_3O_4 Nanostructures and Their Cytotoxicity. *Mater. Res. Express* **2014**, *1*, 015015.

(8) Shi, X.; Gong, H.; Li, Y.; Wang, C.; Cheng, L.; Liu, Z. Graphene-Based Magnetic Plasmonic Nanocomposite for Dual Bioimaging and Photothermal Therapy. *Biomaterials* **2013**, *34*, 4786−4793.

(9) Gao, Y.; Zou, X.; Zhao, J. X.; Li, Y.; Su, X. Graphene Oxide-Based Magnetic Fluorescent Hybrids for Drug Delivery and Cellular Imaging. *Colloids Surf., B* **2013**, *112*, 128−133.

(10) Mao, G. Y.; Yang, W. J.; Bu, F. X.; Jiang, D. M.; Zhao, Z. J.; Zhang, Q. H.; Fang, Q. C.; Jiang, J. S. One-Step Hydrothermal Synthesis of Fe_3O_4@C Nanoparticles with Great Performance in Biomedicine. *J. Mater. Chem. B* **2014**, *2*, 4481−4488.

(11) Yang, Y. Q.; Asiri, A. M.; Tang, Z. W.; Du, D.; Lin, Y. H. Graphene Based Materials for Biomedical Applications. *Mater. Today* **2013**, *16*, 365−373.

(12) Yang, K.; Feng, L.; Hong, H.; Cai, W.; Liu, Z. Preparation and Functionalization of Graphene Nanocomposites for Biomedical Applications. *Nat. Protoc.* **2013**, *8*, 2392−2403.

(13) Zhang, L.; Xia, J.; Zhao, Q.; Liu, L.; Zhang, Z. Functional Graphene Oxide as a Nanocarrier for Controlled Loading and Targeted Delivery of Mixed Anticancer Drugs. *Small* **2010**, *6*, 537−544.

(14) Chu, H. L.; Cheng, T. M.; Chen, H. W.; Chou, F. H.; Chang, Y. C.; Lin, H. Y.; Liu, S. Y.; Liang, Y. C.; Hsu, M. H.; Wu, D. S.; Li, H. Y.; Ho, L. P.; Wu, P. C.; Chen, F. R.; Chen, G. S.; Shieh, D. B.; Chang, C. S.; Su, C. H.; Yao, Z.; Chang, C. C. Synthesis of Apolipoprotein B Lipoparticles to Deliver Hydrophobic/Amphiphilic Materials. *ACS Appl. Mater. Interfaces* **2013**, *5*, 7509−7516.

(15) Swain, A. K.; Bahadur, D. Enhanced Stability of Reduced Graphene Oxide Colloid Using Cross-Linking Polymers. *J. Phys. Chem. C* **2014**, *118*, 9450−9457.

DOI: 10.1021/acsami.5b02536
ACS Appl. Mater. Interfaces 2015, 7, 8013−8022

(16) Luk, B. T.; Zhang, L. Current Advances in Polymer-Based Nanotheranostics for Cancer Treatment and Diagnosis. *ACS Appl. Mater. Interfaces* **2014**, *6*, 21859−21873.
(17) Gong, J.; Huo, M.; Zhou, J.; Zhang, Y.; Peng, X.; Yu, D.; Zhang, H.; Li, J. Synthesis, Characterization, Drug-loading Capacity and Safety of Novel Octyl Modified Serum Albumin Micelles. *Int. J. Pharm.* **2009**, *376*, 161−168.
(18) Ramasamy, T.; Tran, T. H.; Choi, J. Y.; Cho, H. J.; Kim, J. H.; Yong, C. S.; Choi, H. G.; Kim, J. O. Layer-by-Layer Coated Lipid-Polymer Hybrid Nanoparticles Designed for Use in Anticancer Drug Delivery. *Carbohydr. Polym.* **2014**, *102*, 653−661.
(19) Nikam, D. S.; Jadhav, S. V.; Khot, V. M.; Phadatare, M. R.; Pawar, S. H. Study of AC Magnetic Heating Characteristics of $Co_{0.5}Zn_{0.5}Fe_2O_4$ Nanoparticles for Magnetic Hyperthermia Therapy. *J. Magn. Magn. Mater.* **2014**, *349*, 208−213.
(20) Shanta Singh, N.; Kulkarni, H.; Pradhan, L.; Bahadur, D. A Multifunctional Biphasic Suspension of Mesoporous Silica Encapsulated with YVO_4:Eu^{3+} and Fe_3O_4 Nanoparticles: Synergistic Effect Towards Cancer Therapy and Imaging. *Nanotechnology* **2013**, *24*, 065101.
(21) Wang, C.; Wu, C.; Zhou, X.; Han, T.; Xin, X.; Wu, J.; Zhang, J.; Guo, S. Enhancing Cell Nucleus Accumulation and DNA Cleavage Activity of Anti-Cancer Drug via Graphene Quantum Dots. *Sci. Rep.* **2013**, *3*, 2852.
(22) Gurunathan, S.; Han, J. W.; Eppakayala, V.; Jeyaraj, M.; Kim, J. H. Cytotoxicity of Biologically Synthesized Silver Nanoparticles in MDA-MB-231 Human Breast Cancer Cells. *Biomed. Res. Int.* **2013**, *2013*, 535796.
(23) Bhattacharya, K.; Naha, P. C.; Naydenova, I.; Mintova, S.; Byrne, H. J. Reactive Oxygen Species Mediated DNA Damage in Human Lung Alveolar Epithelial (A549) Cells from Exposure to Non-Cytotoxic MFI-Type Zeolite Nanoparticles. *Toxicol. Lett.* **2012**, *215*, 151−160.
(24) Pradhan, L.; Srivastava, R.; Bahadur, D. pH- and Thermosensitive Thin Lipid Layer Coated Mesoporous Magnetic Nanoassemblies as a Dual Drug Delivery System Towards Thermochemotherapy of Cancer. *Acta Biomater.* **2014**, *10*, 2976−2987.
(25) Swain, A. K.; Bahadur, D. Facile Synthesis of Twisted Graphene Solution from Graphite-KCl. *RSC Adv.* **2013**, *3*, 19243−19246.
(26) Delbecq, F.; Kono, F.; Kawai, T. Preparation of PVP−PVA−Exfoliated Graphite Cross-Linked Composite Hydrogels for the Incorporation of Small Tin Nanoparticles. *Eur. Polym. J.* **2013**, *49*, 2654−2659.
(27) Cai, M. C.; Qian, H.; Wei, Z. K.; Chen, J. J.; Zheng, M. S.; Dong, Q. F. Polyvinyl Pyrrolidone-Assisted Synthesis of a Fe_3O_4/Graphene Composite with Excellent Lithium Storage Properties. *RSC Adv.* **2014**, *4*, 6379−6382.
(28) Hoppe, C. E.; Lazzari, M.; Pardinas-Blanco, I.; Lopez-Quintela, M. A. One-Step Synthesis of Gold and Silver Hydrosols Using Poly(*N*-vinyl-2-pyrrolidone) as a Reducing Agent. *Langmuir* **2006**, *22*, 7027−7034.
(29) Shalviri, A.; Raval, G.; Prasad, P.; Chan, C.; Liu, Q.; Heerklotz, H.; Rauth, A. M.; Wu, X. Y. pH-Dependent Doxorubicin Release from Terpolymer of Starch, Polymethacrylic Acid and Polysorbate 80 Nanoparticles for Overcoming Multi-Drug Resistance in Human Breast Cancer Cells. *Eur. J. Pharm. Biopharm.* **2012**, *82*, 587−597.
(30) Yao, X.; Chen, L.; Chen, X.; Zhang, Z.; Zheng, H.; He, C.; Zhang, J.; Chen, X. Intracellular pH-Sensitive Metallo-Supramolecular Nanogels for Anticancer Drug Delivery. *ACS Appl. Mater. Interfaces* **2014**, *6*, 7816−7822.
(31) Jaiswal, M. K.; De, M.; Chou, S. S.; Vasavada, S.; Bleher, R.; Prasad, P. V.; Bahadur, D.; Dravid, V. P. Thermoresponsive Magnetic Hydrogels as Theranostic Nanoconstructs. *ACS Appl. Mater. Interfaces* **2014**, *6*, 6237−6247.
(32) Guo, D.; Zhu, L.; Huang, Z.; Zhou, H.; Ge, Y.; Ma, W.; Wu, J.; Zhang, X.; Zhou, X.; Zhang, Y.; Zhao, Y.; Gu, N. Anti-Leukemia Activity of PVP-Coated Silver Nanoparticles Via Generation of Reactive Oxygen Species and Release of Silver Ions. *Biomaterials* **2013**, *34*, 7884−7894.
(33) An, Q.; Sun, C.; Li, D.; Xu, K.; Guo, J.; Wang, C. Peroxidase-Like Activity of Fe_3O_4@carbon Nanoparticles Enhances Ascorbic Acid-Induced Oxidative Stress and Selective Damage to PC-3 Prostate Cancer Cells. *ACS Appl. Mater. Interfaces* **2013**, *5*, 13248−13257.
(34) Shukla, R. K.; Sharma, V.; Pandey, A. K.; Singh, S.; Sultana, S.; Dhawan, A. ROS-Mediated Genotoxicity Induced by Titanium Dioxide Nanoparticles in Human Epidermal Cells. *Toxicol. in Vitro* **2011**, *25*, 231−241.
(35) Maeda, H.; Bharate, G. Y.; Daruwalla, J. Polymeric Drugs for Efficient Tumor-Targeted Drug Delivery Based on EPR-Effect. *Eur. J. Pharm. Biopharm.* **2009**, *71*, 409−419.
(36) Jaiswal, M. K.; Pradhan, A.; Banerjee, R.; Bahadur, D. Dual pH and Temperature Stimuli-Responsive Magnetic Nanohydrogels for Thermo-Chemotherapy. *J. Nanosci. Nanotechnol.* **2014**, *14*, 4082−4089.
(37) Zhang, W.; Guo, Z.; Huang, D.; Liu, Z.; Guo, X.; Zhong, H. Synergistic Effect of Chemo-Photothermal Therapy Using PEGylated Graphene Oxide. *Biomaterials* **2011**, *32*, 8555−8561.
(38) Sahu, N. K.; Singh, N. S.; Pradhan, L.; Bahadur, D. Ce^{3+} Sensitized $GdPO_4$:Tb^{3+} with Iron Oxide Nanoparticles: A Potential Biphasic System for Cancer Theranostics. *Dalton Trans.* **2014**, *43*, 11728−11738.
(39) Kundu, J.; Chung, Y. I.; Kim, Y. H.; Tae, G.; Kundu, S. C. Silk Fibroin Nanoparticles for Cellular Uptake and Control Release. *Int. J. Pharm.* **2010**, *388*, 242−250.

DOI: 10.1021/acsami.5b02536
ACS Appl. Mater. Interfaces 2015, 7, 8013−8022